Micro-metamaterial antenna characteristics using microring embedded silver bars

A. E. Arumona, A. Garhal, S. Punthawanunt, K. Ray, P. Youplao & P. Yupapin

ONLINE FIRST

Springer

Springer

TECHNICAL PAPER

Micro-metamaterial antenna characteristics using microring embedded silver bars

A. E. Arumona[1,2,3] · A. Garhal[4] · S. Punthawanunt[5] · K. Ray[6] · P. Youplao[7] · P. Yupapin[1,2]

Abstract

A unique micro-metamaterial antenna for light and microwave wavelength conversion is proposed, where the antenna has the form of a panda ring which consists of the mu negative metamaterial silver bars embedded at the microring center. The micro-metamaterial antenna characteristics are investigated, where the antenna resonance frequency and frequency range of 1.60 THz and 1–2.2 THz are achieved. The radiation pattern of the micro-metamaterial antenna is plotted, where the obtained gain and directivity of the antenna are − 8.13 dB. The optimum antenna radiation efficiency is 1 when the antenna has dissipative loss is neglected. The micro-metamaterial antenna can be used as a converter between light and microwave, which is useful for a wavelength converter device.

1 Introduction

A metamaterial is a material that exhibits special properties of light when its geometry is artificially altered. In other words, the arrangement of the structure of a material at nanoscale gives rise to the observation of special properties of light. Metamaterials are classified into four distinct

✉ P. Yupapin
preecha.yupapin@tdtu.edu.vn

A. E. Arumona
arumonaedwardarumona.st@tdtu.edu.vn

1 Computational Optics Research Group, Advanced Institute of Materials Science, Ton Duc Thang University, District 7, Ho Chi Minh City, Vietnam

2 Faculty of Applied Sciences, Ton Duc Thang University, District 7, Ho Chi Minh City, Vietnam

3 Division of Computational Physics, Institute for Computational Science, Ton Duc Thang University, Ho Chi Minh City 700000, Vietnam

4 Amity School of Engineering and Technology, Amity University Rajasthan, Jaipur, India

5 Faculty of Science and Technology, Kasem Bundit University, Bangkok 10250, Thailand

6 Amity School of Applied Sciences, Amity University Rajasthan, Jaipur, India

7 Department of Electrical Engineering, Faculty of Industry and Technology, Rajamangala University of Technology Isan Sakon Nakhon Campus, Sakon Nakhon 47160, Thailand

groups based on the permittivity (ε), and permeability (μ) of these materials. The first group of metamaterials is the Double Positive (DPS) which has $\varepsilon > 0$, and $\mu > 0$. The second group is the epsilon negative (ENG) which has $\varepsilon < 0$, and $\mu > 0$. The third group is the Double Negative (DNG) which has $\varepsilon < 0$, and $\mu < 0$. The last group is the mu negative (MNG) which has $\varepsilon > 0$, and $\mu < 0$ (Fedotov 2017). Rezaeieh et al. (2015) designed a loop antenna that consists of metamaterial MNG unit cells. The electromagnetic region employed for the study is the microwave region. The frequency bandwidth is in the range of 0.64–1.1 GHz corresponding to the wavelength of 0.272–0.468 m. The gain of 3.2 dBi is achieved. Rezaeieh et al. (2017) designed a planar Yagi antenna that consists of MNG metamaterial. The study proposed a novel method to reduce the size of the antenna. The electromagnetic region employed for the study is the microwave region in the frequency range of 0.72–1.48 GHz. The frequency range corresponds to the wavelength of 0.203–0.416 m. The gain of 4.10 dBi is achieved. Jahani et al. (2010) proposed a fabrication technique that is low-cost to reduce the size of circular patch antennas, where the antenna fabricated for the study is formed by two with different helix parameters. The antenna consists of metamaterial MNG. The electromagnetic region employed for the work is the microwave region in the frequency range of 0.4–2 GHz. The frequency range corresponds to the wavelength of 0.149–0.749 m. The first antenna has a gain of − 0.6 dBi, and the second antenna has a gain of − 7.9 dBi. Lee et al. (2018) designed

a compact patch antenna dual bands, where the antenna consists of an MNG metamaterial transmission lines. The antenna is specifically designed for smart helmet applications. The electromagnetic region employed for the study is the microwave region in the frequency range of 2–6 GHz. The frequency range corresponds to the wavelength of 0.050–0.149 m. The radiation efficiency of the antenna is 0.7(70%) while the gain is 8.0 dBi. Simorangkir and Lee (2015) designed a dual-band antenna that consists of an MNG metamaterial transmission line. The study involved both theoretical and experimental work. The theoretical results are in agreement with experimental results. The electromagnetic region for the study is the microwave region in the frequency range of 3–10 GHz. The frequency range corresponds to the wavelength of 0.03–0.10 m. The gain of 6.7 dBi is achieved for the first band while for the second band the gain of 10.3 dBi is achieved. Zhu et al. (2015) designed two novel coplanar antennas that consist of metamaterial MNG transmission lines. The electromagnetic region employed for the study is the microwave region, where the frequency range of 1.5-3 GHz corresponds to the wavelength of 0.1–0.2 m. The first antenna gain is 1.89 dBi while the second antenna gain is 2.78 dBi. The radiation efficiency of 0.7 (70%) is achieved for the first antenna while 0.75(75%) radiation efficiency is achieved for the second antenna. In this present work, micro-antenna that consists of a metamaterial will be designed and the micro-antenna metamaterial characteristics will be studied. The micro-antenna has the form of the panda ring. It consists of silver bars embedded at the center microring. The electromagnetic region for this work is between the microwave region and the optical region. The frequency range of 1–3 THz is employed in this work which corresponds to the wavelength of 100–300 μm. The HFSS software version 13.0 (Ansys Corporation, 2014) which stands for high frequency structure simulator will be employed in the design and simulation of the micro-antenna. HFSS software uses the Finite Element Method (FEM). The Matlab program will be employed for plotting the graphs when parameters are extracted from the HFSS simulation results.

2 Antenna structure and design

The micro-metamaterial antenna in the form of a panda-ring circuit is shown in Fig. 1, where the silver bars are embedded at the center microring. The effective permittivity of the silver bars at center microring is described by the Drude model (Tunsiri et al. 2019; Prince 2018) as given in Eq. (1)
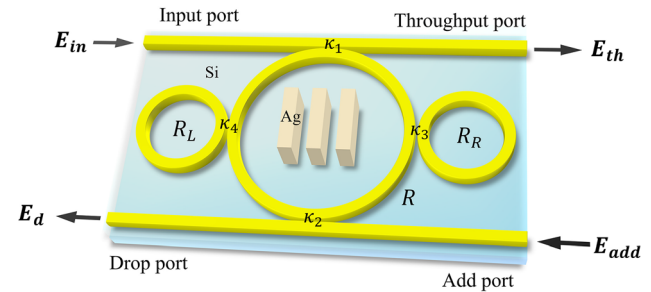

Fig. 1 Illustrates the fabrication structure of the micro-metamaterial antenna, where E_{th} is defined as the throughput port, E_d is defined as the drop port, E_{add} is defined as the add port, E_{in} is defined as the input port. K_1–K_4 are the coupling coefficients

$$\varepsilon_{eff} = 1 - \frac{\omega_p^2}{\omega^2} \tag{1}$$

where the plasma frequency $\left(\omega_p = \left[\frac{ne^2}{\varepsilon_0 m} \right]^{-1/2} \right)$, the electron density, relative permittivity, mass, electron charge are $n_e, \varepsilon_0, m_e, e$, respectively, and ω is electromagnetic wave frequency. The effective permeability of the silver bars at the center microring is given in Eq. (2) (Krzysztofik and Cao 2018) as:

$$\mu_{eff} = 1 - \frac{\left[f_{mp}^2 - f_o^2 \right]}{[f^2 - f_o^2 - j\gamma f]} \tag{2}$$

where f is defined as input signal frequency, f_{mp} is defined as the magnetic plasma frequency, f_o is defined as resonant frequency, and γ is defined as the losses in the medium. The general description of the microring system in Fig. 1 is given in Eq. (3) (Pornsuwancharoen et al. 2017; Prateep et al. 2016) as:

$$E_{th} = m_3 E_{in} + m_3 E_{add} \tag{3}$$

$$E_d = m_5 E_{add} + m_6 E_{in} \tag{4}$$

where E_{th} is defined as the throughput port, E_d is defined as the drop port, E_{add} is defined as the add port, E_{in} is defined as the input port, and the terms m_2, m_3, m_5, m_6 in Eqs. (3 and 4) are defined in the given reference (Pornsuwancharoen et al. 2017; Prateep et al. 2016). The two small rings at the sides of the center microring are the phase modulators and induce the nonlinear effect in the system. The nonlinear Kerr effect is given as $n = n_0 + n_2 I = n_0 + n_2 P/A_{eff}$, where n is the refractive index, n_0 is the linear refractive index, and n_2 is the nonlinear refractive index. Optical intensity and power are I and P respectively. The effective mode core area of the device is A_{eff}. The optical field (E_{in}) enters the system at the input port, where the coupling of light coupled to the linear waveguide and the center microring. The system has two output ports (E_{th}, and E_d). The throughput port can be

connected to optical fiber network via cable connection. The add port (E_{add}) is only used for modulation and multiplexing of signals. The system has been employed for various applications (Arumona et al. 2020a, b; Bunruangses et al. 2019; Garhwal et al. 2020).

For the antenna design, the HFSS software is employed. Firstly, the silver bars at the center of the silicon substrate are simulated as shown in Fig. 2a, where the z and y-axes are the perfect electric and magnetic boundary conditions of the wave-port at the y-axis. The parameters are extracted to calculate the effective permittivity and permeability, where the result of the calculation identifies the class of metamaterial silver bars belongs to in the frequency range of 1-3THz. The method of extraction of parameters employed in this work is well explained in (Numan and Sharawi 2013). The equations involved in the calculation are given in Eqs. (5–8) (Numan and Sharawi 2013) as:

$$z = \pm \sqrt{\frac{(1 + S_{11})^2 - S_{21}^2}{(1 - S_{11})^2 - S_{21}^2}} \tag{5}$$

$$n = (k_o d)^{-1} \left\{ Im\left[In\left(e^{ink_o d}\right) + 2m\pi \right] - iReIn\left(e^{ink_o d}\right) \right\} \tag{6}$$

where $e^{ink_o d} = \frac{S_{21}}{1 - S_{21}\frac{z-1}{z+1}}$, reflection and transmission coefficients are S_{11} and S_{21}. The wave number is $k_o = \frac{2\pi f}{c}$, d is
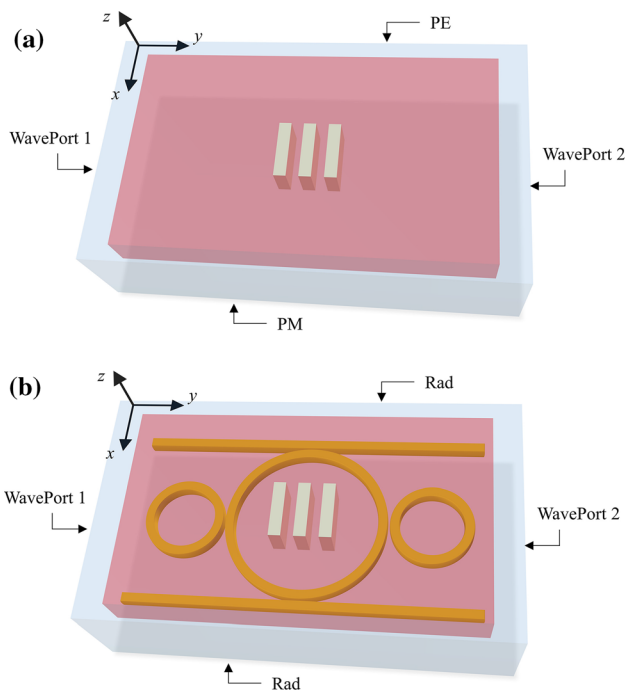

Fig. 2 Ilustration of the HFSS structure, where **a** Silver bars at the center of the silicon substrate inside the radiation box with perfect electric (PE) and magnetic (PM) boundary conditons, **b** Silver bars at the center ring inside the radiation box with radiation (Rad) boundary condition

the substrate thickness, z is the impedance, c is the speed of light, m is the branch index, and n is the refractive index.

$$\varepsilon = \frac{n}{z} \tag{7}$$

$$\mu = nz \tag{8}$$

The dielectric loss tangent (Rogalin et al. 2018) is given as:

$$tan\delta = \frac{1}{\omega \varepsilon_r \varepsilon_o \rho} \tag{9}$$

where ε_r is the dielectric constant, ρ is the resistivity.

The relationship of reflection and transmission coefficients in whispering gallery mode microring (Jan 2004) are given as:

$$S_{11} = |R|^2 \tag{10}$$

$$S_{21} = |T|^2 \tag{11}$$

where R is defined as the reflected field and T is defined as the transmitted field.

3 Results and discussion

The simulation software HFSS is employed to identify the class of metamaterial silver bars at the center of the silicon substrate, as shown in Fig. 2a. The suitable parameters are given in Table 1. The frequency sweep is from 0.1 to 3 THz with a step size of 0.1. The discrete solver is employed to ensure the accuracy of the work. The discrete solver is the most accurate solver in the HFSS software. The silicon substrate has a dielectric loss tangent of 6.85×10^{-5} m^{-1} which is calculated from Eq. (9). The relation between the input and output of the antenna is given by the reflection and transmission coefficients (S_{11} and S_{21}). The reflection coefficient (S_{11}) is also known as the return loss. The return loss gives the measure of how much power is accepted by the antenna at the input port when power is supplied to the antenna. If the S_{11} value is $< - 10$ dB, which indicates that the accepted power is over 90% of the supplied power. If the S_{11} value is $> - 10$ dB, which indicates that the accepted power is less than 90% of the supplied power. If the S_{11} value is 0 dB then no power is accepted by the antenna. The transmission coefficient (S_{21}) is the forward transmission from the input port to the output port and measures the output signal relative to the input signal. The S-parameters (scattering parameters) are extracted from the simulation results following the method described in (Numan and Sharawi 2013). From Eqs. (5–8) the permittivity (ε), and permeability (μ) are calculated and plotted using the Matlab program. The plot of the reflection (S_{11}), and transmission (S_{21}) coefficients

Table 1 The parameters of the micro-metamaterial antenna

Parameters	Symbols	Values	Units
Supplied power	P	1.0	W
Si-linear waveguide length	L	32.0	μm
Si center ring radius	R	7.28	μm
Si small ring radius	R_L	3.50	μm
Si small ring radius	R_R	3.50	μm
Silver dielectric constant	ε_r	1	
Silver bar thickness	d	5.5	μm
Silver bar length	L	7.5	μm
Silver bar width	W	1.5	μm
Coupling coefficient	κ	0.50	
Refractive index Si (Prabhu et al. 2010a, b)	n_{Si}	3.42	
Si nonlinear refractive index (Prabhu et al. 2010a, b)	n_2	1.3×10^{-13}	$m^2 W^{-1}$
Waveguide core effective (Prabhu et al. 2010a, b)	A_{eff}	0.30	$μm^2$
Waveguide loss	α	0.50	$dB\ (cm)^{-1}$
Substrate length	L	26.2	μm
Substrate width	W	37.4	μm
Substrate thickness	d	12.50	μm
Dielectric loss tangent	δ	6.85×10^{-5}	m^{-1}
Si dielectric constant	ε_r	11.9	
Permittivity of free space	ε_o	8.85×10^{-12}	Fm^{-1}
Substrate resistivity (Dai et al. 2004)	ρ	1×10^3	Ωcm

are shown in Fig. 3a–b where the resonance frequency is at 2 THz, and 2.10 THz respectively. The value of S_{11} is − 18.5 dB which is less than − 10 dB which indicates that the accepted power is over 90% of the supplied power. The real part of the permittivity and permeability is plotted in Fig. 4a where the permittivity is positive ($\varepsilon > 0$) while the
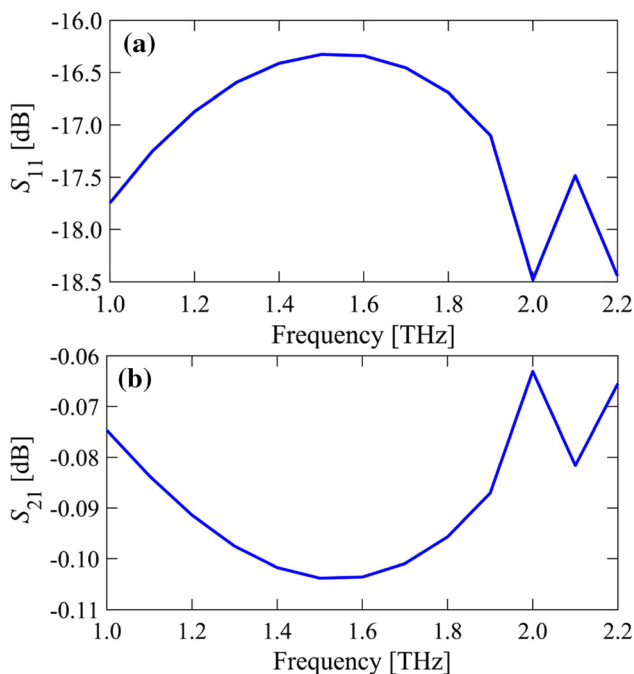

Fig. 3 Plots of the S-parameters extracted from the HFSS software, where (a) reflection coefficient, (b) transmission coefficient where the resonance frequency is 2THz and 2.10THz, respectively
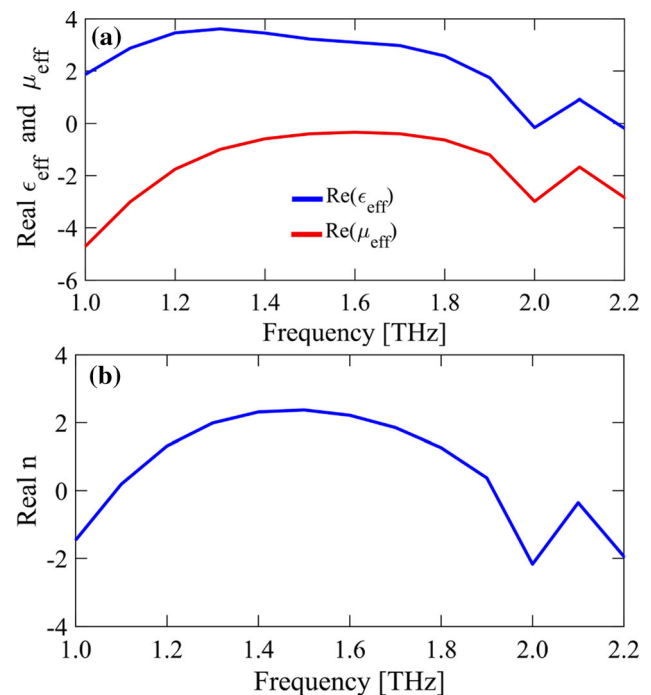

Fig. 4 Results of the Matlab program, where **a** real permittivity and permeability, **b** real refractive index where the resonance frequency is 2THz

permeability is negative ($\mu < 0$) as clearly shown in the graph. The resonance frequency for the applied permittivity and permeability is 2 THz. The real part of the refractive index is shown in Fig. 4b which shows the resonance frequency of 2 THz. The refractive index is negative at this resonance frequency. The results for the permittivity, permeability, and refractive index ($\varepsilon > 0, \mu < 0,$ and $n < 0$) indicates that the silver bar belongs to the MNG metamaterial group. The silver bars embedded at the center microring with two small rings at the sides of the center microrings are shown in Fig. 2b. The radiation boundary condition is employed to study the micro-metamaterial antenna characteristics. The simulation results are shown in Figs. 6, 7 and 8. The reflection (S_{11}) and transmission (S_{21}) coefficients resonance frequency is 1.6THz, as shown in Fig. 5a, b. The value of S_{11} is − 6 dB, which is higher than − 10 d, which indicates that the receiver power is lower than 90% of the supplied power. The radiation pattern of the micro-metamaterial antenna is shown in Fig. 6a–c, where gain, directivity, and radiation efficiency are plotted, respectively. The type of radiation pattern of the antenna is the directional radiation pattern. The total gain and directivity of the antenna are shown in Fig. 7a, b. The gain and directivity have the same value of − 8.13 dB. The radiation efficiency of the micro-metamaterial antenna is shown in Fig. 7c which is 1. This is expected for the radiation efficiency when the gain and directivity are equal. The
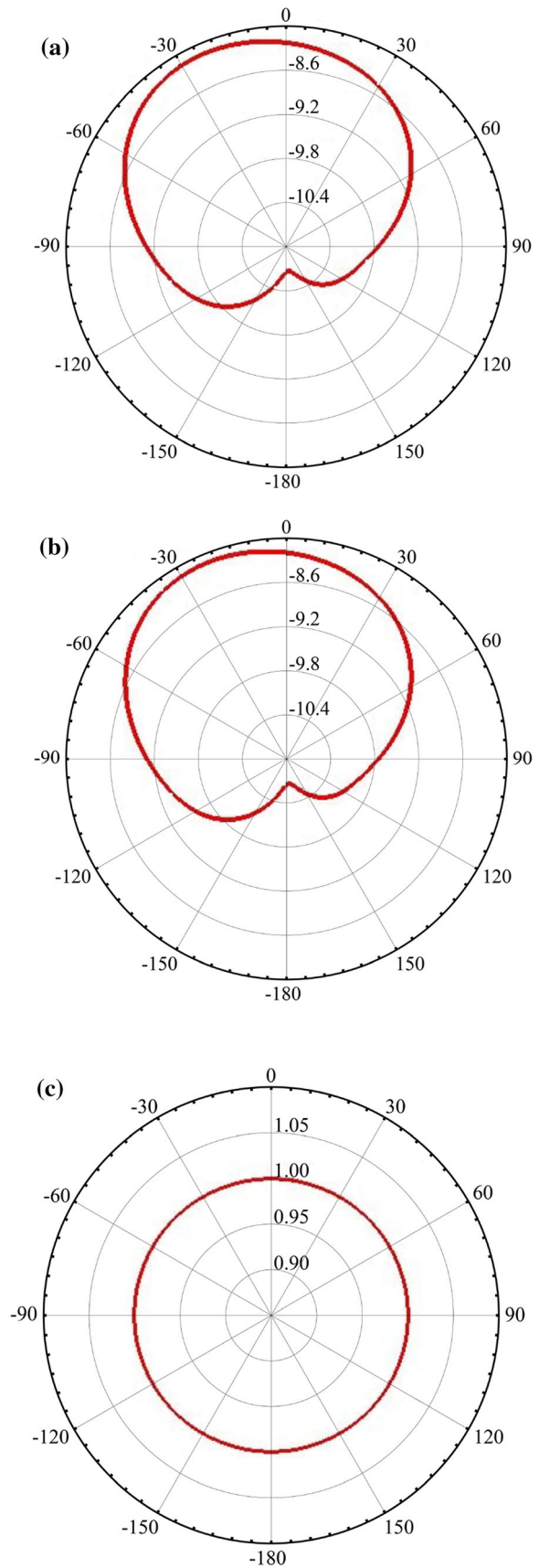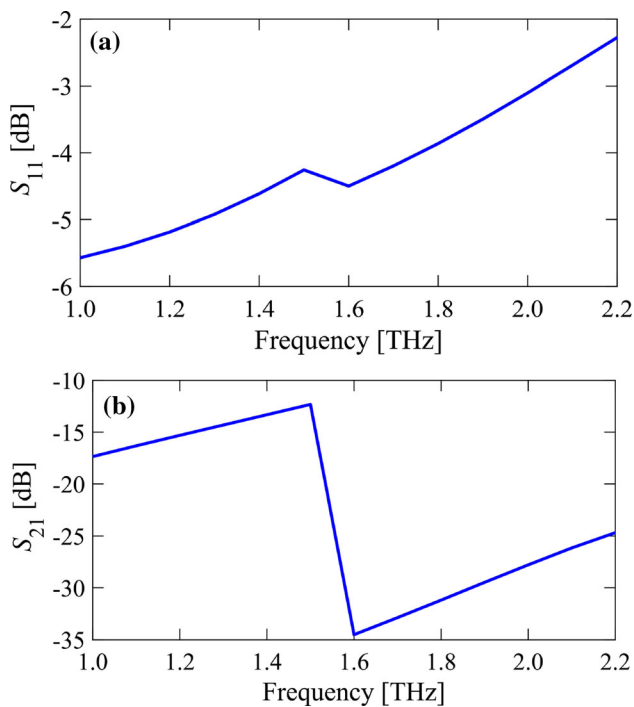

Fig. 5 Plots of the antenna S-parameters extracted and plotted using the Matlab program, where (a) the reflection coefficient, (b) transmission coefficient. Both having a resonance frequency of 1.60THz

Fig. 6 Plots of the antenna radiation pattern plot of **a** the gain, **b** the directivity, **c** the radiation efficiency
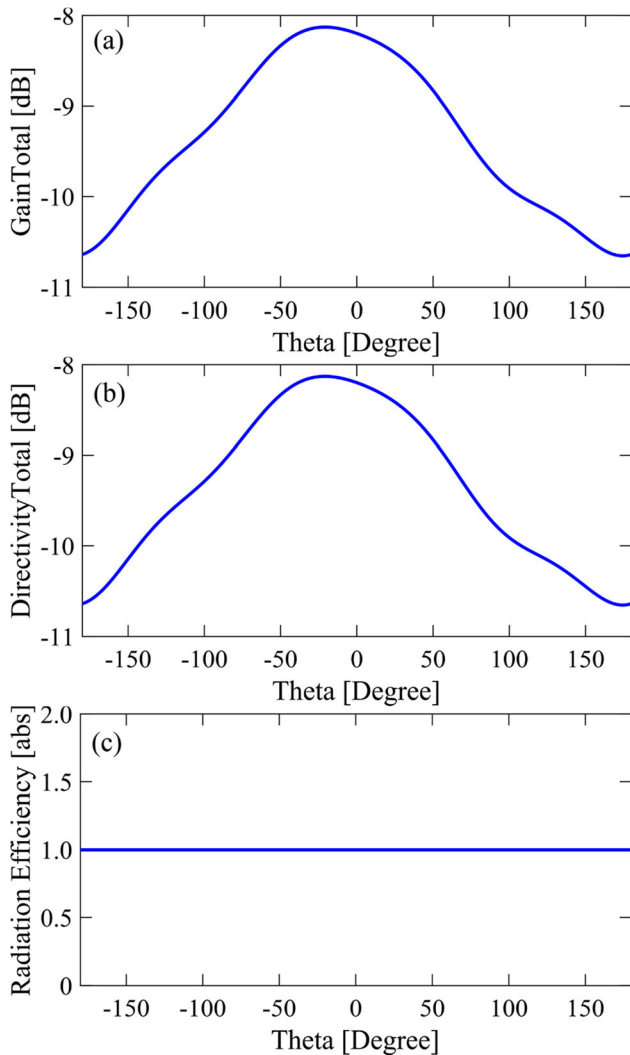

Fig. 7 The plot of **a** the total gain of the antenna, **b** the total directivity of the antenna, and **c** the radiation efficiency of the antenna. The gain and directivity is -8.13 dB while the radiation efficiency is 1

results of Fig. 7a–c indicate that the micro-metamaterial antenna does not suffer from dissipative losses. Dissipative loss (I^2R) is responsible for the low radiation efficiency of most antennas. The low gain and directivity can be employed by devices that require low gain and directivity for its operations. The mobile cellular network requires low directivity for its operation. The micro-metamaterial antenna operates in the region between microwave and optical regions. This system can be utilized as a converter. That is, to convert signals at the microwave region to signals at the optical region. The system can easily be

connected to a fiber network through the output port (E_{th}) as a cable connection to an optical network. The center microring can be utilized for LiFi and WiFi networks, which are the wireless connections. This is made possible by employing the whispering gallery mode (WGM) (Punthawanunt et al. 2018) as shown in Fig. 8. Figure 8a is the whispering gallery mode (WGM) formed at the center microring. The WGM results from the trapping of light inside the microring which is made possible by the non-linearity effect in the system induced by the two small rings at the sides of the center microring. Figure 8b is the electric field distribution across the system.

4 Conclusion

The micro-metamaterial antenna characteristics are investigated for lightwave and microwave wavelength conversion by employing the HFSS software. The Optiwave result of WGM is also applied. The micro-metamaterial is the MNG metamaterial silver bars embedded at the center microring forms the micro-antenna structure. The silvers are driven by the WGM, where the micro-metamaterial antenna resonance frequency of 1.60 THz, with the
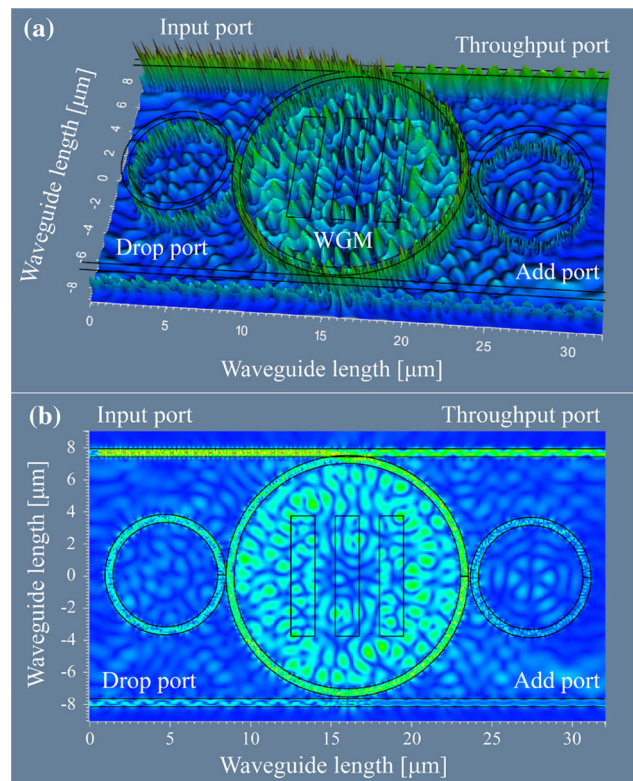

Fig. 8 Shows the Optiwave results of the system in Fig. 1 using the selected parameters in Table 1, where **a** whispering gallery mode formed at the center ring, where WGM, **b** electric field distribution across the system

directional radiation pattern, is achieved and characterized. The obtained optimum gain and directivity are − 8.13 dB. In this work, the micro-antenna dissipative loss is not included. The gain and directivity are the same values, which are equal to 1. The proposed antenna is a compacted circuit, which can be fabricated and applied in realistic applications. Antenna propagation is formed at the center circuit, while the cable connection can be connected via the circuit ports. The micro-metamaterial antenna can be employed for a wireless network by the propagation at the centering. It can be connected to the optical fiber network via cable connection and operate in the microwave-optical wavelength (frequency) conversion, where the potential of communication, sensors, quantum communication and spectroscopy can be applied.

References

Ansys Corporation, "HFSS" (2014) Suite v13, Pittsburg (PA), USA

Arumona AE, Amiri IS, Punthawanunt S et al (2020) High-density quantum bits generation using microring plasmonic antenna. Opt Quantum Electron 52, Article ID 208

Arumona AE, Amiri IS, Yupapin P (2020b) Plasmonic micro-antenna characteristics using gold grating embedded panda-ring circuit. Plasmonics 15:279–285

Bunruangses M, Youplao P, Amiri IS et al (2019) Brain sensor and communication model using plasmonic microring antenna network. Opt Quantum Electron 51, Article ID 349

Dai J, Zhang J, Zhang W et al (2004) Terahertz time-domain spectroscopy characterization of the far-infrared absorption and index of refraction of high-resistivity, float-zone silicon. J Opt Soc Am B 21(7):1379–1386

Fedotov V (2017) Metamaterials. In: Kasap S, Capper P (eds) Springer handbook of electronics and photonic materials. Springer handbooks. Springer, Cham, pp 1351–1362

Garhwal A, Ray K, Arumona AE et al (2020) Spin-wave generation using MZI embedded plasmonic antenna for quantum communications. Opt Quantum Electron 52, Article ID 241

Jahani S, Rashed-Mohassel J, Shahabadi M (2010) Miniaturization of circular patch antennas using MNG metamaterials. IEEE Antennas Wirel Propag 9:1194–1196

Jan KT (2004) Nonlinear optics in ultra-high Q whispering gallery optical microcavities. Dissertation (Ph.D). California Institute of Technology, U.S.A. https://resolver.caltech.edu/CaltechETD:etd-06072004-085555

Krzysztofik WJ, Cao TN (2018) Metamaterials in application to improve antenna parameters. In: Metamaterial and Metasurfaces, pp 63–85. Josep Canet-Ferrer Intechopen. https://doi.org/10.5772/intechopen.80636

Lee H, Yang H, Myeong S et al (2018) Dual-band MNG patch antenna for smart helmet. Electron Lett 54(19):1101–1102

Numan AB, Sharawi MS (2013) Extraction of material parameters for metamaterials using a full-wave simulator. IEEE Antennas Propag Mag 55(5):202–211

Pornsuwancharoen N, Amiri IS, Suhailin FH et al (2017) Micro-current source generated by a WGM of light within a stacked silicon-graphene-Au waveguide. IEEE Photon Technol Lett 29:1768–1771

Prabhu AM, Tsay A, Han Z et al (2010a) Extreme miniaturization of silicon add-drop microring filters for VLSI photonics applications. IEEE Photon J 2:436–444

Prabhu AM, Alan T, Zhanghua H et al (2010b) Extreme miniaturization of silicon add-drop microring filters for VLSI photonics applications. IEEE Photon J 2(3):436–444

Prateep P, Surasak C, Yupapin P (2016) Analytical and simulation of a triple micro whispering gallery mode probe system for a 3D blood flow rate sensor. Appl Opt 55:9504–9513

Prince G (2018) Controlling level splitting by strong coupling of surface plasmon resonances with rhodamine-6G on a gold grating. Plasmonics 13:2067–2077

Punthawanunt S, Aziz MS, Phatharacorn P et al (2018) Lifi cross-connection node model using whispering gallery mode of light in a microring resonator. Microsyst Technol 24:4833–4838

Rezaeieh SA, Antoniades MA, Abbosh AM (2015) Compact wide-band loop antenna partially loaded with mu-negative metamaterial unit-cells for directivity enhancement. IEEE Antenna Wirel Propag 15:1893–1896

Rezaeieh SA, Antoniades MA, Abbosh AM (2017) Miniaturization of planar Yagi antennas using mu-negative metamaterial-loaded reflector. IEEE Trans Antenna Propag 65(12):6827–6837

Rogalin VE, Kaplunov IA, Kropotov GI (2018) Optical Materials for the THz Range. Opt Spectrosc 125(6):1053–1064

Simorangkir RBVB, Lee Y (2015) A planar dual-band periodic leaky-wave antenna based on a mu-negative (MNG) transmission line. IEEE Trans Antennas Propag 63(5):2370–2374

Tunsiri S, Nopparat T, Thanunchai T et al (2019) Microring switching control using plasmonic ring resonator circuits for super-channel use. Plasmonics 14:1669–1677

Zhu L, Gao XJ, Wang GM et al (2015) Novel compact asymmetric coplanar strip (ACPS)-fed zeroth-order resonant antennas with bandwidth enhancement. Freq Berl 69(7–8):311–316